



Cite this: DOI: 10.1039/d1bm00157d

# Nano-enabled coordination platform of bismuth nitrate and cisplatin prodrug potentiates cancer chemoradiotherapy *via* DNA damage enhancement†

Yin-Chu Ma,<sup>‡a</sup> Xin-Feng Tang,<sup>‡b</sup> You-Cui Xu,<sup>b</sup> Wei Jiang,<sup>a</sup> Yong-Jie Xin,<sup>a</sup> Wei Zhao,<sup>a</sup> Xu He,<sup>a</sup> Li-Gong Lu<sup>‡\*a</sup> and Mei-Xiao Zhan<sup>\*a</sup>

The combination of chemotherapy and radiotherapy (chemoradiotherapy) is a promising strategy, extensively studied and applied clinically. Meanwhile, radiosensitizers play an important role in improving clinical radiotherapy therapeutic efficacy. There are still some disadvantages in practical applications, because radiosensitizers and drugs are difficult to deliver spatio-temporally to tumor sites and work simultaneously with low efficiency for DNA damage and repair inhibition, leading to an inferior synergistic effect. Herein, a suitable radiosensitizer of nano-enabled coordination platform (NP@PVP) with bismuth nitrate and cisplatin prodrug is developed by a simple synthetic route to improve the effectiveness of chemo-radiation synergistic therapy. When NP@PVP is internalized by a tumor cell, the bismuth in NP@PVP can sensitize radiation therapy (RT) by increasing the amount of reactive oxygen species generation to enhance DNA damage after X-ray radiation; meanwhile, the cisplatin in NP@PVP can inhibit DNA damage repair with spatio-temporal synchronization. NP@PVP is demonstrated to exhibit higher sensitization enhancement ratio (SER) of 2.29 and excellent tumor ablation capability upon irradiation *in vivo* in comparison with cisplatin (SER of 1.78). Our strategy demonstrates that the RT sensitization effect of bismuth and cisplatin based NP@PVP has great anticancer potential in chemo-radiation synergistic therapy, which is promising for clinical application.

Received 28th January 2021,

Accepted 12th March 2021

DOI: 10.1039/d1bm00157d

rsc.li/biomaterials-science

## Introduction

Radiation therapy (RT) is the main treatment for various types of cancers clinically, and up to 50% of cancer patients receive this treatment modality.<sup>1–4</sup> RT can effectively kill cancer cells by destroying the DNA double strand, but the self-repair mechanism of DNA in cancer cells highly limits its therapeutic effect.<sup>5–7</sup> In addition, the insensitivity of hypoxic tumors to RT and the inevitable side effects at therapeutic doses also limit its efficacy.<sup>8–10</sup> Meanwhile, normal tissues can also be injured like cancerous tissues because of non-selective absorption of X-rays. Thence, there are major problems caused by RT that

need to be overcome with great efforts. High-efficiency radiosensitizers are important factors for improving RT efficacy, and it is very important to design new effective radiosensitizers for enhancing the absorption of X-rays, thereby achieving an effective therapeutic effect below the safe dose.<sup>11</sup>

Previous studies reported radiosensitizers based on nanomaterials, such as upconverting nanoparticles,<sup>12</sup> polyoxometalates,<sup>13</sup> WS<sub>2</sub>,<sup>14</sup> TaOx,<sup>15</sup> gold nanoparticles,<sup>16</sup> and bismuth based nanomaterials,<sup>17–22</sup> which mainly achieved good results in RT enhancement by high-Z atoms. Among them, bismuth based nanomaterials have attracted widespread attention due to their significant radiation dose enhancement under kilovolt X-rays, which is much higher than that of the well-known radiation sensitizers of gold nanoparticles.<sup>23–27</sup> Bismuth has an extremely high X-ray attenuation coefficient, which is ideal as a foundation for the design of new effective radiosensitizers. Furthermore, compared with other heavy metal elements, bismuth is one of the cheapest and most biocompatible elements. Its compounds (*e.g.* colloidal bismuth subcitrate) have already been used as clinical drugs for gastrointestinal disease treatment.<sup>28</sup> However, in most cases, effective tumor

<sup>a</sup>Zhuhai Interventional Medical Center, Zhuhai Precision Medical Center, Zhuhai People's Hospital, Zhuhai Hospital Affiliated with Jinan University, Zhuhai 519000, China. E-mail: zhanmeixiao1987@126.com, luligong1969@jnu.edu.cn

<sup>b</sup>School of Life Sciences, University of Science and Technology of China, Hefei 230027, China

†Electronic supplementary information (ESI) available. See DOI: 10.1039/d1bm00157d

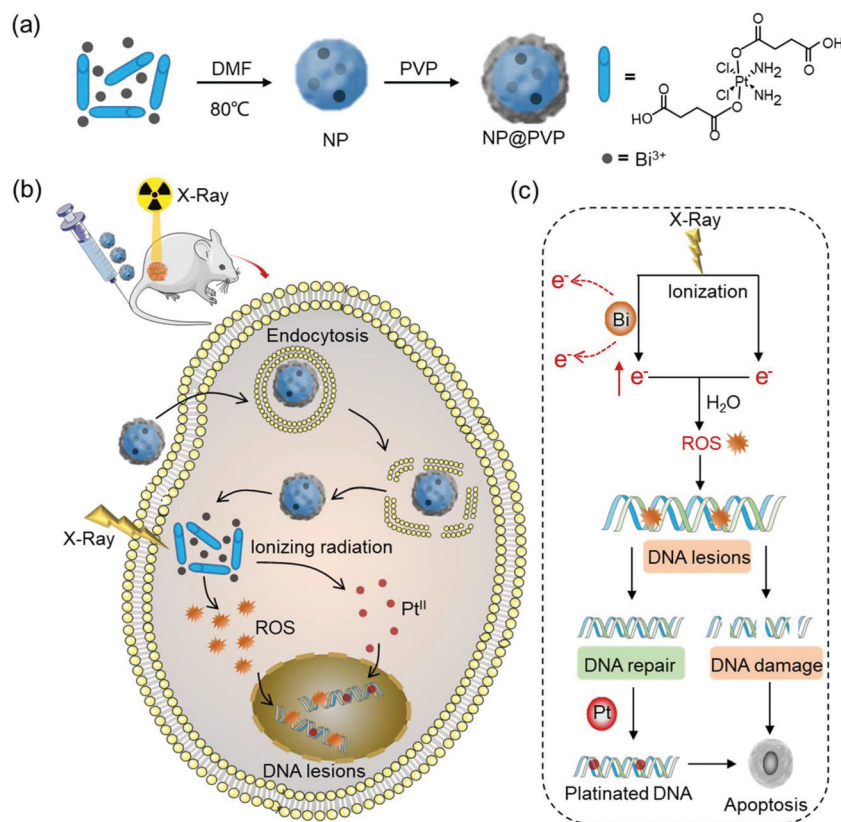
‡These authors contributed equally to this work.

clearance cannot be achieved only by a single therapy, and it is even easy to cause adverse effects such as drug resistance, increasing the difficulty of tumor treatment.<sup>29–31</sup> It is particularly important to note that the DNA damage to the tumor after RT will be repaired promptly, thereby reducing the effectiveness of the treatment. In addition, by using modified bismuth based nanomaterials as radiation sensitizers, RT can be combined with other types of treatment strategies for synergistic therapy in tumors. Therefore, it is necessary to find a new treatment strategy to cope with this problem. As a result, the most promising strategy to improve the efficacy of RT is to develop new effective radiosensitizers and combine them with other therapies to achieve synergistic treatment.<sup>32</sup>

Chemotherapy, as an enduring treatment strategy in clinical tumor therapy, is suitable to be combined with RT to achieve effective tumor removal. Platinum drugs are used in 80% of clinical treatment programs, accounting for 50% of all anti-cancer drugs used clinically, which are some of the most significant categories in chemotherapy.<sup>33–36</sup> It is worth mentioning that cisplatin is one of the most used platinum drugs, which can generate highly toxic reactive oxygen species (ROS; e.g.  $\cdot\text{OH}$ ) by enzyme activations.<sup>37–40</sup> And so far, the combination of chemotherapy and radiotherapy, which is also known as chemo-radiotherapy, has been applied to a variety of cancers and regarded as a main treatment method. In recent

years, nanocarrier-based chemo-radiotherapy has attracted great attention, which has advantages in promoting drug tumor accumulation and retention to improve chemo-radiotherapy efficacy. However, there are still some shortcomings in chemo-radiotherapy practical applications: radiosensitizers and drugs are difficult to spatio-temporally deliver to tumor sites, and work simultaneously with low efficiency in inhibiting DNA damage and repair, resulting in poor synergy.

Herein, we develop a suitable nanomedicine with radiosensitizer and drug of a nano-enabled coordination platform (NP@PVP) with bismuth and cisplatin prodrug to improve the effectiveness of chemo-radiation synergistic therapy with X-ray radiation. As shown in Scheme 1a, NP@PVP is succinctly constructed by cisplatin prodrug (*c,c,t*-[Pt(NH<sub>3</sub>)<sub>2</sub>Cl<sub>2</sub>(OOCCH<sub>2</sub>CH<sub>2</sub>COOH)<sub>2</sub>], HOOC–Pt–COOH), Bi(NO<sub>3</sub>)<sub>3</sub>, and polyvinylpyrrolidone (PVP) *via* a facile synthesis to ensure bismuth and cisplatin achieve synchronization in time and space. NP@PVP including bismuth and cisplatin is delivered to the tumor sites in the same time and space and internalized by the tumor cells. The bismuth in NP@PVP can sensitize RT by increasing the amount of ROS generation to enhance DNA damage after X-ray radiation; meanwhile, the cisplatin in NP@PVP can cause DNA damage and inhibit DNA damage repair with synchronization spatio-temporally. The bioplatfom of NP@PVP could also enhance the tumor accumulation and



**Scheme 1** Schematic representation for (a) the facile synthesis of nano-enabled coordination platform (NP@PVP) with bismuth and cisplatin prodrug and (b, c) the mechanism of enhanced chemo-radiotherapy efficacy under X-ray irradiation.

retention to a large extent. Subsequently, NP@PVP based on bismuth and cisplatin prodrug has remarkable X-ray sensitization capability, which not only enhanced DNA damage but also decreased DNA repair caused by generation of ROS, and exhibits great anticancer potential of chemo-radiation synergistic therapy (Schemes 1b and c).

## Experimental

### ROS detection of NP@PVP after X-ray irradiation

EMT-6 cells (murine breast cancer cell line,  $10^5$  cells per well) were seeded in 24-well plates (Guangzhou Jet Bio-Filtration Co. Ltd) and cultured for 12 h. The cells were incubated with medium containing cisplatin or NP@PVP with an equivalent Pt dose of  $2 \mu\text{g mL}^{-1}$ . After 6 h, the cells were irradiated with X-rays (5 Gy) and incubated with DCFH-DA ( $10 \mu\text{M}$ ) for another 20 min. The cells were fixed with paraformaldehyde and stained with DAPI (blue signal). ROS (green signal) was detected with a confocal laser scanning microscope (Nikon HD25).

### *In vivo* tumor inhibition study

All animal procedures were performed in accordance with the Guidelines for Care and Use of Laboratory Animals of the University of Science and Technology of China (USTC) and approved by the Animal Ethics Committee of the USTC (Animal Ethical and Welfare Number: USTCACUC1901022). Tumor-bearing mice were divided to 3 groups when the volume of tumors reached  $100 \text{ mm}^3$ . The mice of every group were intravenously injected with PBS, cisplatin, and NP@PVP at a dose of  $2 \text{ mg kg}^{-1}$  Pt. After 12 h, five of the mice of each group received X-ray irradiation of 5 Gy. The tumor volume was

monitored by measuring lengths and widths of the tumors with a vernier caliper every 3 days and calculated by the following formula: tumor volume ( $\text{mm}^3$ ) =  $0.5 \times \text{width}^2 \times \text{length}$ . The weight of each mouse was also measured every three days. At the end of the tumor suppression study, the tumors were excised and stained with hematoxylin and eosin (H&E), and the blood of mice was collected and centrifuged to obtain the serum, which was used to detect the level of biochemical indices of liver functional enzymes.

## Results and discussion

NP@PVP was constructed by the reaction method described in the ESI.† As shown in the transmission electron microscope (TEM) image, NP@PVP exhibited a well-dispersed nanostructure. The hydrodynamic diameter of NP@PVP was measured with dynamic light scattering (DLS), which was about 190 nm as shown in Fig. 1a. Furthermore, X-ray photoelectron spectroscopy (XPS) analysis was used to determine the elemental composition and chemical valence of NP@PVP. As shown in Fig. 1b, the XPS spectrum confirmed the existence of Bi and Pt elements in NP@PVP. X-ray energy dispersive spectroscopy (EDS) was also used to determine the composition of NP@PVP. The EDS elemental analysis showed that the weight proportion of Bi and Pt elements was 40.11% and 22.78%, respectively (Fig. 1c). The weight ratio of Bi and Pt in NP@PVP was also determined by inductively coupled plasma mass spectrometry. The results indicated a ratio of about 2 : 1 (Bi : Pt), which was in line with the EDS results. High-resolution TEM images (Fig. 1d) showed that NP@PVP had a high degree of crystallinity with lattice fringes of 0.33 and 0.20 nm, which were related to (012) plane of the rhombohedral Bi phase and

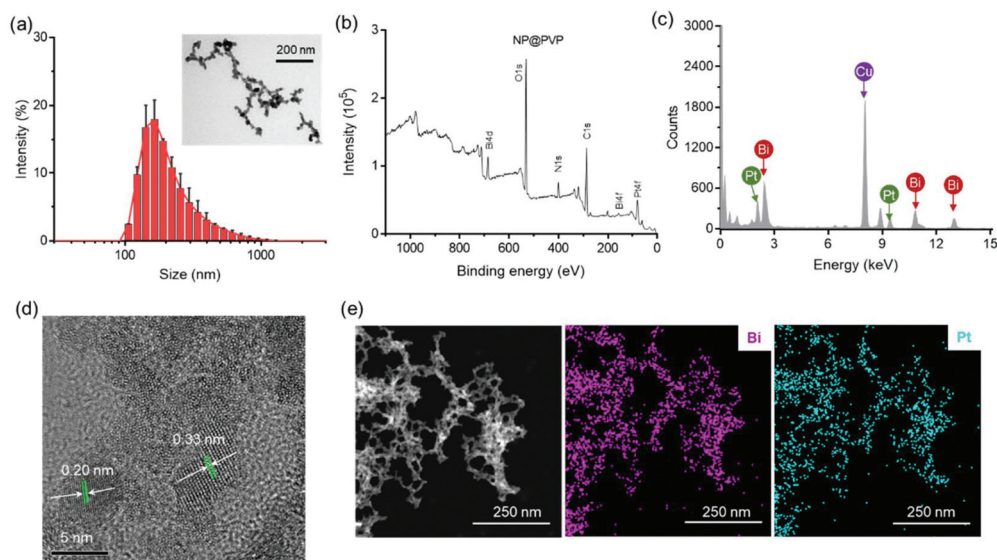


**Fig. 1** Synthesis strategy and structural characterization of NP@PVP. (a) Hydrodynamic diameter measured by DLS and corresponding TEM image of NP@PVP. (b) XPS spectrum of NP@PVP. (c) EDS analysis of NP@PVP. (d) High-resolution TEM image of NP@PVP. (e) HAADF-STEM image and EDS element scanning maps of NP@PVP.

(023) planes of crystalline  $\text{Bi}_2\text{O}_3$ , respectively. The microstructure of NP@PVP was further determined by elemental mapping and high angle annular dark field scanning transmission electron microscopy (HAADF-STEM) (Fig. 1e), from which it was clear to see that Bi and Pt elements were distributed on NP@PVP.

To investigate the cellular internalization of NP@PVP, we first developed Cy5-loaded NP@PVP, named NP@PVP/Cy5, to detect the amount of NP@PVP in EMT-6 murine breast cancer cells by fluorescence-activated cell sorting. After EMT-6 cells were incubated with NP@PVP/Cy5 for different times, the signal of Cy5 in the cells was measured. As shown in Fig. 2a, the fluorescent signal intensity of Cy5 in the cells gradually increased with the extension of the incubation time. There were no significant differences of cell uptake after 4 h and 6 h of incubation as evidenced by similar mean fluorescence intensity (MFI) of Cy5 (Fig. 2b). We also used NP@PVP/Cy5 to measure the fluorescence intensity in cells to investigate NP@PVP uptake using confocal laser scanning microscopy (CLSM). It was found that cells treated with NP@PVP/Cy5 showed stronger fluorescence at 4 h and 6 h with no significant difference, which confirmed the excellent cell internalization

ability of NP@PVP (Fig. 2c and d). The chemotherapy effect mediated by NP@PVP and cisplatin (the concentration of Pt was  $0\text{--}5\ \mu\text{g mL}^{-1}$ ) was measured with EMT-6 cells using MTT assays (Fig. 2e). As expected, enhanced cell cytotoxicity was noticed with an increase of Pt concentration of NP@PVP. The viability of EMT-6 cells was also no different after being treated with NP@PVP or cisplatin at the same Pt concentration, confirming that nanoparticles made from cisplatin prodrugs still had cytotoxicity.

We further investigated the mechanisms of NP@PVP-mediated enhanced radio-sensitization. According to reports in the literature, the formation of ROS plays a key role in RT after ionizing radiation.<sup>39</sup> On the one hand, strongly generated ROS might attack the DNA covalent bonds, leading to apoptosis or programmed cell death. On the other hand, ROS could fix with  $\text{O}_2$  to cause DNA radicals ( $\text{DNA}^{\cdot}$ ), leading to formation of much more stable DNA peroxides ( $\text{DNA-OO}^{\cdot}$ ) to prevent lesion repair.<sup>36</sup> After 6 h incubation of NP@PVP or cisplatin, the cells were irradiated with or without X-ray (5 Gy) and incubated with DCFH-DA ( $10\ \mu\text{M}$ ) for another 20 min. ROS generation (green signal) was detected by using CLSM. As shown in Fig. 3a and b, there was similar weak green signal among the

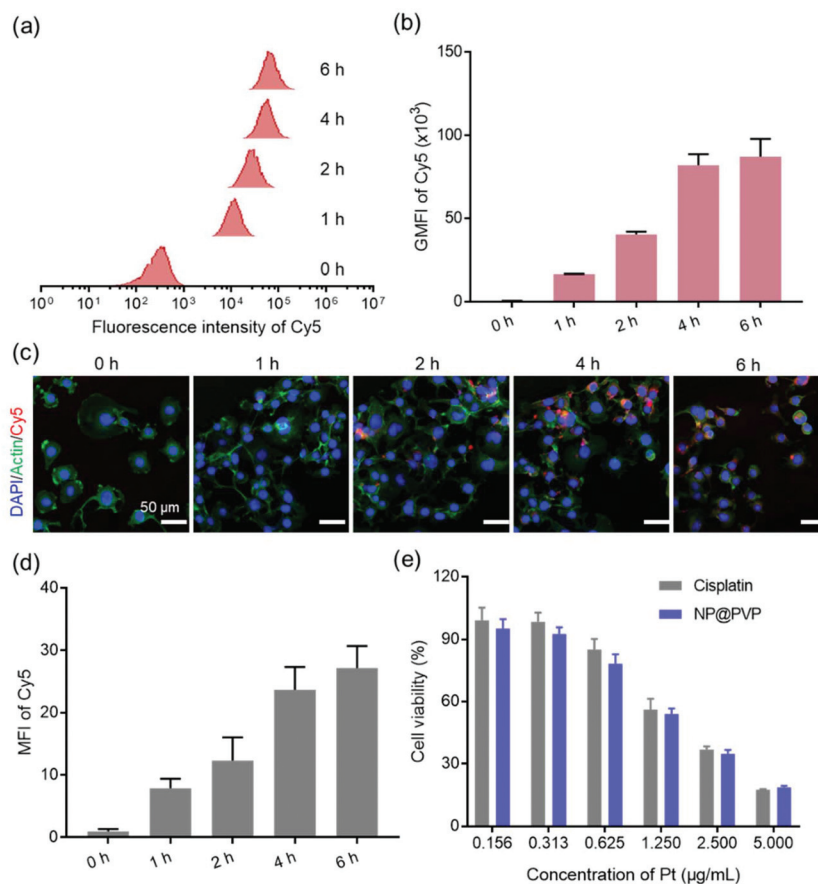


**Fig. 2** The cellular uptake and cytotoxicity of NP@PVP. Cellular uptake of NP@PVP/Cy5 in EMT-6 cells measured by flow cytometry analysis (a) and laser scanning confocal microscopy (c). Relative GMFI analyses of cellular uptake of NP@PVP/Cy5 in EMT-6 cells measured by flow cytometry analysis (b) and laser scanning confocal microscopy (d). (e) Viability of EMT-6 cells after incubation with different concentrations of NP@PVP or cisplatin.

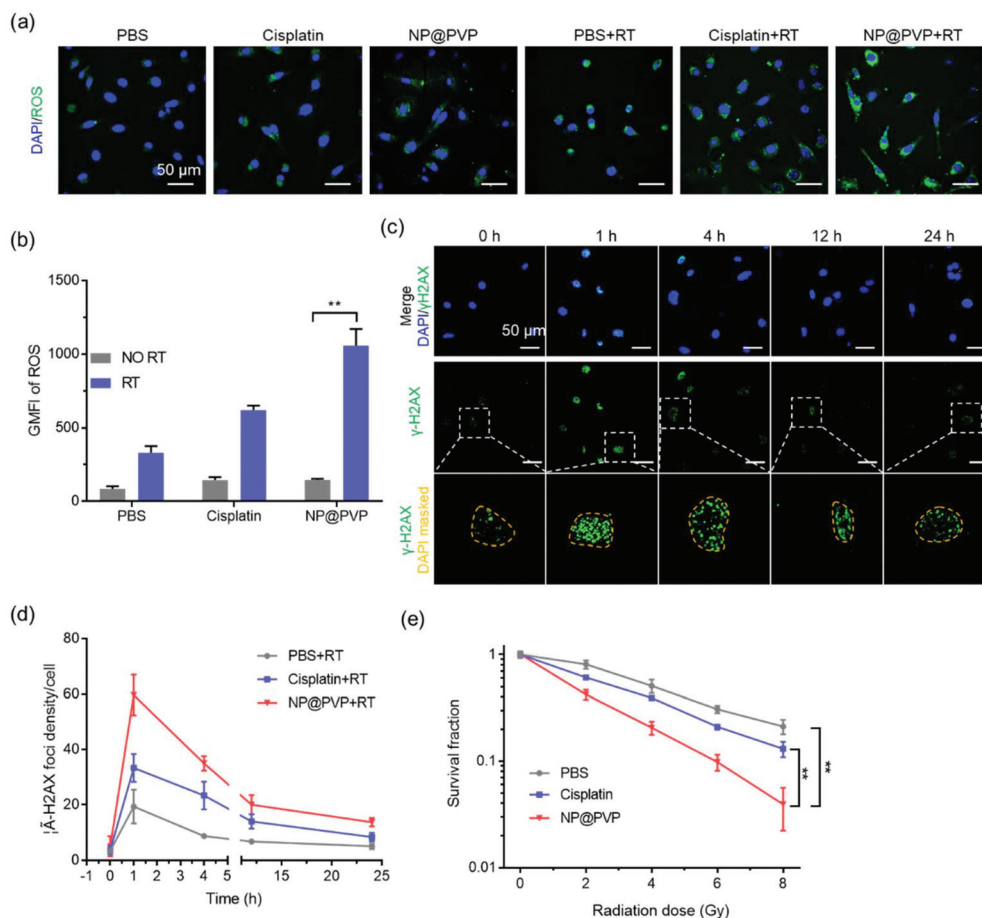


**Fig. 3** *In vitro* NP@PVP enhanced ROS and DNA damage after X-ray irradiation. (a) ROS detected by fluorescence spectra of DCF in cells treated with PBS, cisplatin, NP@PVP, PBS + RT, cisplatin + RT, and NP@PVP + RT (the concentration of Pt was  $2 \mu\text{g mL}^{-1}$ ). (b) MFI of ROS detected by fluorescence spectra of DCF in cells treated with PBS, cisplatin, NP@PVP, PBS + RT, cisplatin + RT, and NP@PVP + RT. (c) Phosphor-histone 2AX ( $\gamma$ -H2AX) staining in cells treated with NP@PVP + RT. (d) Quantitative analysis of  $\gamma$ -H2AX foci density in cells treated with PBS + RT, cisplatin + RT, and NP@PVP + RT (the dose of X-rays was 5 Gy). (e) Survival fraction of EMT-6 cells treated with X-ray radiation (0, 2, 4, 6, and 8 Gy) after being pretreated with PBS, cisplatin, and NP@PVP for 6 h. Data are shown as the mean  $\pm$  SD ( $n = 3$ ). \*\* $P < 0.01$ .

groups of Pt and NP@PVP, indicating Pt and NP@PVP both caused only a slight generation of ROS. Interestingly, compared with the cells without RT, cellular green fluorescence signal was enhanced after RT. Furthermore, the ROS level in the cells treated with NP@PVP and RT increased by 1.89-fold and 3.21-fold compared with the control group (PBS) and the group treated with Pt and RT, proving that bismuth-based NP@PVP with remarkable X-ray sensitization capability could enhance the formation of radicals involving ROS after RT.

We further evaluated DNA double-strand breaks after cells were treated with RT by immunofluorescent labeling for phosphor-histone 2AX ( $\gamma$ -H2AX) foci.<sup>38</sup> The EMT-6 cells were irradiated by X-ray at a dose of 5 Gy after being pretreated with cisplatin or NP@PVP (the concentration of Pt was  $2 \mu\text{g mL}^{-1}$ ) for 6 h, and incubated for another 0, 1, 4, 12, and 24 h for  $\gamma$ -H2AX immunofluorescent staining. As shown in Fig. 3c and S1,<sup>†</sup> compared with the group treated with RT-cisplatin, the rapid accumulation of  $\gamma$ -H2AX foci showed that obvious DNA damage occurred in the cells treated with RT-NP@PVP, con-

firmed the excellent capability of bismuth-based NP@PVP after RT to produce DNA damage. For cells treated with RT alone, the number of  $\gamma$ -H2AX foci decreased sharply over time because of efficient DNA repair mechanism in tumor cells. Furthermore, the number of  $\gamma$ -H2AX foci in the cells treated with NP@PVP and RT exhibited a slow decreasing tendency and was higher than that of the group treated with cisplatin and RT for all times, confirming that the bismuth in NP@PVP can sensitize RT by increasing the amount of ROS generation for enhancing DNA damage after X-ray irradiation. Meanwhile, the cisplatin in NP@PVP could inhibit the DNA damage repair with spatio-temporal synchronization (Fig. 3d).

To further investigate the X-ray sensitization activity of NP@PVP, we assessed the inhibitory effects on colony formation *via* assays of EMT-6 cells. The cells were radiated with 0, 2, 4, 6, and 8 Gy X-rays after being pretreated with PBS, cisplatin, and NP@PVP for 6 h. 7 days later, the cell colonies were counted to evaluate the clonogenic capacities. From the clonogenic assay results in Fig. 3e and S2,<sup>†</sup> NP@PVP significantly

inhibited cell colony formation under X-ray irradiation of 2, 4, and 8 Gy compared with the group of cisplatin. As the dose of X-rays increased, the survival fraction of cells treated with NP@PVP declined slowly and cells treated with cisplatin decreased sharply. For instance, the cell survival fraction pre-treated with NP@PVP decreased to 57.8%, 79.4%, 90.2%, and 96.1% after receiving 2, 4, 6, and 8 Gy X-ray radiation. Meanwhile, the corresponding calculated sensitization enhancement ratio values of cisplatin and NP@PVP groups were 1.78 and 2.29, respectively.

We used the Xenogen IVIS<sup>®</sup> Lumina system to evaluate pharmacokinetics and biodistribution of NP@PVP *in vivo*. The pharmacokinetics *in vivo* was revealed in mice bearing EMT-6 tumors with intravenous (i.v.) injection of NP@PVP/Cy5 (Fig. 4a and b). The blood was taken from orbital venous plexus of mice at various time points post-injection of NP@PVP/Cy5 and centrifuged to collect the plasma for Cy5 signal detection. After NP@PVP/Cy5 injection, the Cy5 content in mice decreased with time, which was almost 0.59% of injection dose at 24 h. The tumor accumulation of NP@PVP/Cy5 was detected by the Xenogen IVIS<sup>®</sup> Lumina system. The amount of Cy5 fluorescence reduced sharply after free Cy5

injection. However, the fluorescent signal gradually increased with time and reached maximum fluorescence at 12 h after NP@PVP/Cy5 injection, attributed to the EPR effect of NP@PVP (Fig. 4c and S3<sup>†</sup>).

Furthermore, after 12 h injection of NP@PVP or cisplatin, the mice were not irradiated or irradiated with X-rays (5 Gy) and DCFH-DA (5 mg kg<sup>-1</sup>) was i.v. injected for another 20 min. The ROS generation (green signal) was detected by using CLSM. As shown in Fig. 4d and e, the tumors treated with NP@PVP + RT showed strong green fluorescence signal (DCF), which was higher than that of the groups treated with cisplatin + RT and NP@PVP. This phenomenon indicated that bismuth and cisplatin based NP@PVP could effectively sensitize RT by increasing the amount of ROS generation to enhance DNA damage after X-ray irradiation.

Encouraged by the superior performance of the RT sensitization effect of bismuth element in NP@PVP *in vitro*, we further investigated the anticancer potential of chemo-radiation therapy using NP@PVP. The mice bearing EMT-6 tumors were divided into 6 groups randomly and received different treatments with PBS (I), PBS + RT (II), cisplatin (III), cisplatin + RT (IV), NP@PVP (V), or NP@PVP + RT (VI) (2 mg kg<sup>-1</sup> of Pt and 5

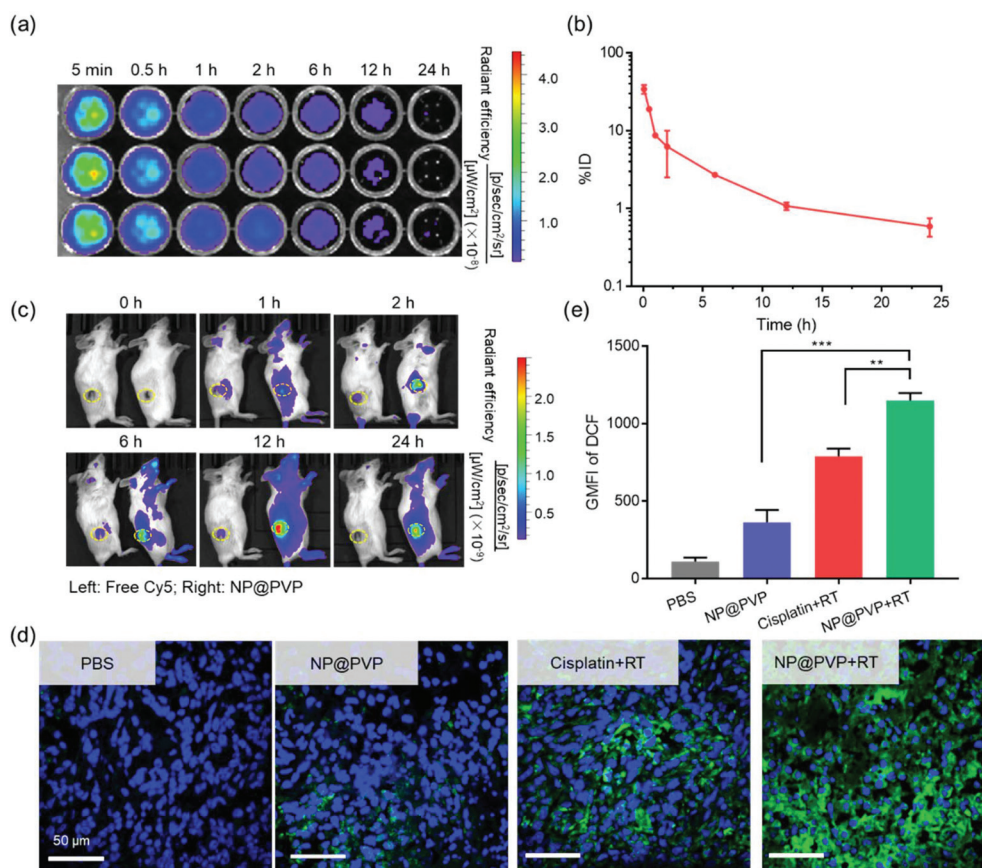


**Fig. 4** Biodistribution and tumor accumulation of NP@PVP *in vivo*. (a) Fluorescence images of serum after intravenous (i.v.) injection of NP@PVP/Cy5. (b) Blood circulation curve of NP@PVP/Cy5 after i.v. injection ( $n = 3$  per group). (c) Fluorescence images of mice after i.v. injection of Cy5 or NP@PVP/Cy5. (d) Images of ROS generation *in vivo*. (e) Corresponding DCF fluorescence intensity of tumors after being treated with PBS, NP@PVP, cisplatin + RT and NP@PVP + RT. The error bars represent the means  $\pm$  SD. \*\* $P < 0.01$ , \*\*\* $P < 0.001$ .

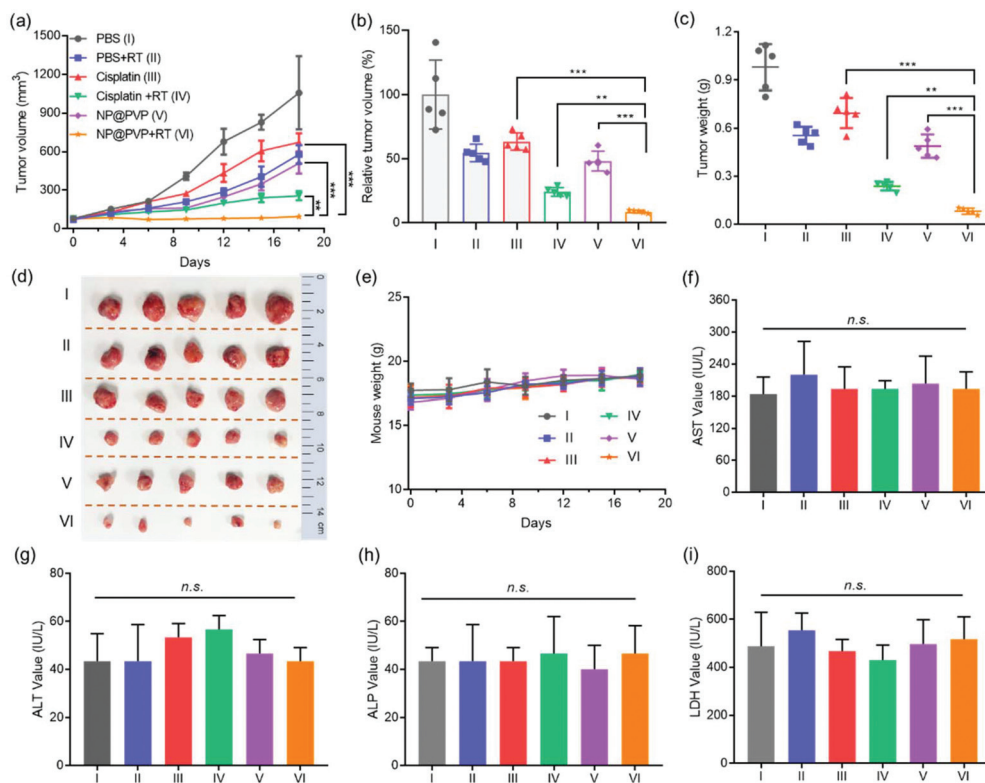


**Fig. 5** Excellent tumor inhibition of NP@PVP *in vivo*. (a) Tumor growth changes of mice and (b) tumor inhibition ratio with various treatments of PBS (I), PBS + RT (II), cisplatin (III), cisplatin + RT (IV), NP@PVP (V), and NP@PVP + RT (VI). Tumor weight (c) and pictures of the tumors (d) after treatments. (e) Mice body weights during the antitumor therapy period. The value of aspartate aminotransferase (AST; f), alanine aminotransferase (ALT; g), alkaline phosphatase (ALP; h), and lactate dehydrogenase (LDH; i) in mice after antitumor treatment. Data are shown as the mean  $\pm$  SD ( $n = 5$ ), \*\* $P < 0.01$ , \*\*\* $P < 0.001$ .

Gy of X-ray radiation). The tumor size increased fast in the PBS group (group I), which was regarded as the control group. The tumor of mice showed growth inhibition for single chemotherapy of cisplatin (group III) and NP@PVP (group V), the values being 36.5% and 51.9% suppression efficiency *versus* the control group. When the mice received PBS + RT (II) with X-ray radiation of 5 Gy, the tumors showed 45.4% growth inhibition. The tumor growth of mice receiving cisplatin + RT (IV) was inhibited by 75.9%, due to the chemo-radiation therapy. As expected, the strongest anticancer effect was observed in mice treated with NP@PVP + RT (91.2% growth inhibition, group VI) indicating that the superior performance of the RT sensitization effect of bismuth based NP@PVP had great anticancer potential of chemo-radiation therapy. According to the results above, the tumors treated with NP@PVP + RT showed significant inhibition, due to the bismuth in NP@PVP sensitizing RT by increasing the amount of ROS generation to enhance DNA damage after X-ray irradiation; meanwhile, the cisplatin in NP@PVP can cause DNA damage and inhibit DNA damage repair with spatio-temporal synchronization. At the end of antitumor therapy, the tumors were collected for weighing and photographing (Fig. 5a and b). As shown in Fig. 5c and d, it was further found that NP@PVP + RT (VI) had the highest suppression efficiency of tumor growth. The antitumor

efficacies of the different treatments were further assessed by H&E staining (Fig. S4<sup>†</sup>). While the tumors in cisplatin (III)- or NP@PVP (V)-treated mice were only partially destroyed, the tumor cells were severely affected after being treated with NP@PVP + RT (VI). The weight of mice was monitored during the therapy period, which showed no significant changes after treatments due to bio-safety (Fig. 5e). The blood of mice was collected when the antitumor therapy finished, which was used to examine the effects of liver functions after the different treatments of the mice. As shown in Fig. 5f-i, the values of aspartate aminotransferase (AST), alanine aminotransferase (ALT), alkaline phosphatase (ALP), and lactate dehydrogenase (LDH) reflecting liver function were measured and showed no obvious changes after treatments, indicating high safety.<sup>41</sup> These results demonstrated that NP@PVP + RT had no detectable side effects for mice, showing the good safety of this chemo-radiotherapy.

## Conclusions

In summary, we have successfully described a strategy to develop a nano-enabled coordination platform based on bismuth and cisplatin prodrug to improve the effectiveness of

chemo-radiation synergistic therapy. The bismuth in NP@PVP can sensitize RT by increasing the amount of ROS generation to enhance DNA damage after X-ray irradiation; meanwhile, the cisplatin in NP@PVP can cause DNA damage and inhibit DNA damage repair with synchronization spatio-temporally. In addition, mice treated with NP@PVP in combination with RT showed the strongest anticancer effect. Taken together, such a strategy demonstrated that the superior performance of the RT sensitization effect of bismuth and cisplatin in NP@PVP had great potential for anticancer chemo-radiation synergistic therapy, which was promising for clinical application.

## Conflicts of interest

There are no conflicts of interest to declare.

## Acknowledgements

This work is supported by the Guangdong Basic and Applied Basic Research Foundation (2020A1515111059), National Key Research and Development Program of China (2017YFA0205200), China Postdoctoral Science Foundation (2019TQ0399 and 2020M673044), and the Fundamental Research Funds for the Central Universities (WK2070000160).

## Notes and references

- G. Erel-Akbaba, L. A. Carvalho, T. Tian, M. Zinter, H. Akbaba, P. J. Obeid, E. A. Chiocca, R. Weissleder, A. G. Kantarci and B. A. Tannous, *ACS Nano*, 2019, **13**, 4028–4040.
- E. C. Ko and S. C. Formenti, *Int. J. Radiat. Biol.*, 2019, **95**, 936–939.
- C. Grassberger, S. G. Ellsworth, M. Q. Wilks, F. K. Keane and J. S. Loeffler, *Nat. Rev. Clin. Oncol.*, 2019, **16**, 729–745.
- X. J. Cheng, Y. Yong, Y. H. Dai, X. Song, G. Yang, Y. Pan and C. C. Ge, *Theranostics*, 2017, **7**, 4087–4098.
- T. Hellday, E. Petermann, C. Lundin, B. Hodgson and R. A. Sharma, *Nat. Rev. Cancer*, 2008, **8**, 193–204.
- S. Goel, D. Ni and W. Cai, *ACS Nano*, 2017, **11**, 5233–5237.
- L. Wen, L. Chen, S. Zheng, J. Zeng, G. Duan, Y. Wang, G. Wang, Z. Chai, Z. Li and M. Gao, *Adv. Mater.*, 2016, **28**, 5072–5079.
- X. Dong, R. Cheng, S. Zhu, H. Liu, R. Zhou, C. Zhang, *et al.*, A heterojunction structured  $W_{0.9}Se_2$  nanoradiosensitizer increases local tumor ablation and checkpoint blockade immunotherapy upon low radiation dose, *ACS Nano*, 2020, **14**, 5400–5416.
- F. Mao, L. Wen, C. Sun, S. Zhang, G. Wang, J. Zeng, *et al.*, Ultrasmall biocompatible  $Bi_2Se_3$  nanodots for multimodal imaging-guided synergistic radiophotothermal therapy against cancer, *ACS Nano*, 2016, **10**, 11145–11155.
- D. Huo, S. Liu, C. Zhang, J. He, Z. Zhou, H. Zhang and Y. Hu, *ACS Nano*, 2017, **11**, 10159–10174.
- D. Luo, A. Johnson, X. Wang, H. Li, B. O. Erokwu, S. Springer, J. Lou, G. Ramamurthy, C. A. Flask and C. Burda, *Nano Lett.*, 2020, **20**, 7159–7167.
- W. Fan, B. Shen, W. Bu, F. Chen, K. Zhao, S. Zhang, L. Zhou, W. Peng, Q. Xiao and H. Xing, *J. Am. Chem. Soc.*, 2013, **135**, 6494–6503.
- Y. Yong, C. Zhang, Z. Gu, J. Du, Z. Guo, X. Dong, J. Xie, G. Zhang, X. Liu and Y. Zhao, *ACS Nano*, 2017, **11**, 7164–7176.
- Y. Yong, X. Cheng, T. Bao, M. Zu, L. Yan, W. Yin, C. Ge, D. Wang, Z. Gu and Y. Zhao, *ACS Nano*, 2015, **9**, 12451–12463.
- G. S. Song, Y. Y. Chen, C. Liang, X. Yi, J. J. Liu, X. Q. Sun, S. D. Shen, K. Yang and Z. Liu, *Adv. Mater.*, 2016, **28**, 7143.
- X. D. Zhang, Z. Luo, J. Chen, X. Shen, S. Song, Y. Sun, S. Fan, F. Fan, D. T. Leong and J. Xie, *Adv. Mater.*, 2014, **26**, 4565–4568.
- G. Song, C. Liang, X. Yi, Q. Zhao, L. Cheng, K. Yang and Z. Liu, *Adv. Mater.*, 2016, **28**, 2716–2723.
- J. M. Kinsella, R. E. Jimenez, P. P. Karmali, A. M. Rush, V. R. Kotamraju, N. C. Gianneschi, E. Ruoslahti, D. Stupack and M. J. Sailor, *Angew. Chem., Int. Ed.*, 2011, **50**, 12308–12311.
- H. Huang, L. Z. He, W. H. Zhou, G. B. Qu, J. H. Wang, N. Yang, J. Gao, T. F. Chen, P. K. Chu and X. F. Yu, *Biomaterials*, 2018, **171**, 12–22.
- M. Ma, Y. Huang, H. R. Chen, X. Q. Jia, S. G. Wang, Z. Z. Wang and J. L. Shi, *Biomaterials*, 2015, **37**, 447–455.
- N. Yu, Z. J. Wang, J. L. Zhang, Z. X. Liu, B. Zhu, J. Yu, M. F. Zhu, C. Peng and Z. G. Chen, *Biomaterials*, 2018, **161**, 279–291.
- X. J. Yu, A. Li, C. Z. Zhao, K. Yang, X. Y. Chen and W. W. Li, *ACS Nano*, 2017, **11**, 3990–4001.
- A. Al Zaki, D. Joh, Z. L. Cheng, A. L. B. De Barros, G. Kao, J. Dorsey and A. Tsourkas, *ACS Nano*, 2014, **8**, 104–112.
- K. L. Ai, Y. L. Liu, J. H. Liu, Q. H. Yuan, Y. Y. He and L. H. Lu, *Adv. Mater.*, 2011, **23**, 4886–4891.
- S. Badrigilan, J. Choupani, H. Khanbabaee, M. Hoseini-Ghahfarokhi, T. J. Webster and L. Tayebi, *Adv. Healthcare Mater.*, 2020, **9**, 1901695.
- R. Zhou, H. Wang, Y. Yang, C. Zhang, X. Dong, J. Du, L. Yan, G. Zhang, Z. Gu and Y. Zhao, *Biomaterials*, 2019, **189**, 11–22.
- J. Liu, X. P. Zheng, L. Yan, L. J. Zhou, G. Tian, W. Y. Yin, L. M. Wang, Y. Liu, Z. B. Hu, Z. J. Gu, C. Y. Chen and Y. L. Zhao, *ACS Nano*, 2015, **9**, 696–707.
- J. M. Kinsella, R. E. Jimenez, P. P. Karmali, A. M. Rush, V. R. Kotamraju, N. C. Gianneschi, E. Ruoslahti, D. Stupack and M. J. Sailor, *Angew. Chem., Int. Ed.*, 2011, **50**, 12308–12311.
- L. Deng, D. Sheng, M. Liu, L. Yang, H. Ran, P. Li, X. Cai, Y. Sun and Z. Wang, *Biomater. Sci.*, 2020, **8**, 858–870.
- Y. Zheng, D. J. Ffuntung, P. Ayotte and L. Sanche, *Radiat. Res.*, 2008, **169**, 481–482.

- 31 L. Huang, Z. J. Li, Y. Zhao, Y. W. Zhang, S. Wu, J. Z. Zhao and G. Han, *J. Am. Chem. Soc.*, 2016, **138**, 14586–14591.
- 32 Y. Dou, Y. Guo, X. Li, X. Li, S. Wang, L. Wang, G. Lv, X. Zhang, H. Wang, X. Gong and J. Chang, *ACS Nano*, 2016, **10**, 2536–2548.
- 33 R. G. Kenny and C. J. Marmion, *Chem. Rev.*, 2019, **119**, 1058–1137.
- 34 R. van der Meel, E. Sulheim, Y. Shi, F. Kiessling, W. J. M. Mulder and T. Lammers, *Nat. Nanotechnol.*, 2019, **14**, 1007–1017.
- 35 T. C. Johnstone, K. Suntharalingam and S. J. Lippard, *Chem. Rev.*, 2016, **116**, 3436–3486.
- 36 X. Y. Wang, X. H. Wang and Z. J. Guo, *Acc. Chem. Res.*, 2015, **48**, 2622–2631.
- 37 W. Jiang, Q. Li, Z. C. Zhu, Q. Wang, J. X. Dou, Y. M. Zhao, W. F. Lv, F. Zhong, Y. D. Yao, G. Q. Zhang, H. Liu, Y. C. Wang and J. Wang, *ACS Appl. Mater. Interfaces*, 2018, **10**, 35734–35744.
- 38 S. J. Kim, J. H. Hur, C. Park, H. J. Kim, G. S. Oh, J. N. Lee, S. J. Yoo, S. K. Choe, H. S. So, D. J. Lim, S. K. Moon and R. Park, *Exp. Mol. Med.*, 2015, **47**, e142.
- 39 W. Jiang, Q. Li, L. Xiao, J. X. Dou, Y. Liu, W. H. Yu, Y. C. Ma, X. Q. Li, Y. Z. You, Z. T. Tong, H. Liu, H. Liang, L. G. Lu, X. D. Xu, Y. D. Yao, G. Q. Zhang, Y. C. Wang and J. Wang, *ACS Nano*, 2018, **12**, 5684–5698.
- 40 P. A. Ma, H. H. Xiao, C. Yu, J. H. Liu, Z. Y. Cheng, H. Q. Song, X. Y. Zhang, C. X. Li, J. Q. Wang, Z. Gu and J. Lin, *Nano Lett.*, 2017, **17**, 928–937.
- 41 Y. Ma, Y. Zhao, N. K. Bejjanki, X. Tang, W. Jiang, J. Dou, M. I. Khan, Q. Wang, J. Xia and H. Liu, *ACS Nano*, 2019, **13**, 8890–8902.